A MECHANISM FOR SPONTANEOUS SELF-PERPETUATING VOLCANISM ON THE TERRESTRIAL PLANETS

P. J. TACKLEY
Seismological Laboratory
Division of Geological and Planetary Sciences
California Institute of Technology
Pasadena, California 91125, USA

D. J. STEVENSON
Division of Geological and Planetary Sciences
California Institute of Technology
Pasadena, California 91125, USA

ABSTRACT. We present a model for self-perpetuating magmatism resulting from Rayleigh-Taylor like instabilities developing spontaneously in regions that are partially molten, or at the solidus. The mechanism is capable of generating large volumes of magma without the need of a plume, or other deep source. Numerical models have been used to determine characteristic timescales, spacings and eruption rates in terms of nondimensional parameters. Scaled to realistic parameter space, the results correspond to timescales and eruption rates compatible with observations of small-scale intra-plate volcanism. Applications to oceanic seamount production, volcano spacing and rapid lithospheric erosion are discussed.

1. Introduction

Volcanoes occur in diverse forms on the Earth's surface. However, they are usually attributed to one of two distinct causes: plate-boundary effects (spreading centers, back-arcs), and deep mantle plumes. Several separate arguments lead to the conclusion that deep mantle plumes reaching the base of the lithosphere must exceed a certain minimum size; these are, diapirs arising from D" exhibit a characteristic size (Griffiths, 1986; Olson et al., 1987), weak plumes may get swept up by the large-scale flow (Boss and Sacks, 1985; Richards and Griffiths, 1988), and weak plumes cannot penetrate phase changes (Liu et al., 1991) and possible chemical boundaries (Kellogg, 1991) in the mantle. However, intra-plate volcanism is observed to have a broad spectrum of sizes, ranging down to small (100s of meters high) seamounts. Hence an alternative mechanism for intra-plate volcanism is required. This argument is reinforced by recent observations of Venus by the Magellan spacecraft. Hundreds of mainly small (<100km diameter) features, probably volcanic in origin, and probably too small to be caused by deep mantle plumes, have been observed.

In this paper we present a novel mechanism, previously proposed by Stevenson (1988), for the production of such intra-plate volcanism. The mechanism involves Rayleigh-Taylor instabilities developing spontaneously in regions of the asthenosphere which are partially molten, or at the onset of melting. The emphasis in this paper is on an understanding of the

D. B. Stone and S. K. Runcorn (eds.),
Flow and Creep in the Solar System: Observations, Modeling and Theory, 307–321.

basic concepts and physics, and an identification of the important parameters and their effects, by means of numerical models and physical argument.

2. Description of the Instability

2.1. GEOMETRY AND INSTABILITY

Figure 1 shows schematically the unstable initial condition which may be representative of, for example, young oceanic lithosphere and asthenosphere. By 'lithosphere' we refer to rock which is over three orders of magnitude more viscous than the asthenosphere, rendering it effectively immobile to asthenospheric flow. With realistic temperature-dependent viscosity the base of this viscous lithosphere corresponds to a geotherm about 300°C lower than the asthenospheric temperature, i.e. typically 1000°C.

As a first approximation, a simple univariant solidus is assumed. The geotherm, which is adiabatic at great depth, intersects the solidus at some lesser depth. Phase equilibria between solid and melt buffer the temperature at the solidus temperature or 'wet adiabat' above this depth, until the influence of the cold upper boundary causes the temperature profile to depart from this wet adiabat and drop steeply to the surface (following approximately an error function in the case of oceanic lithosphere). D, the distance between the depth of onset of melting and the base of the viscous lithosphere, is the most important length scale.

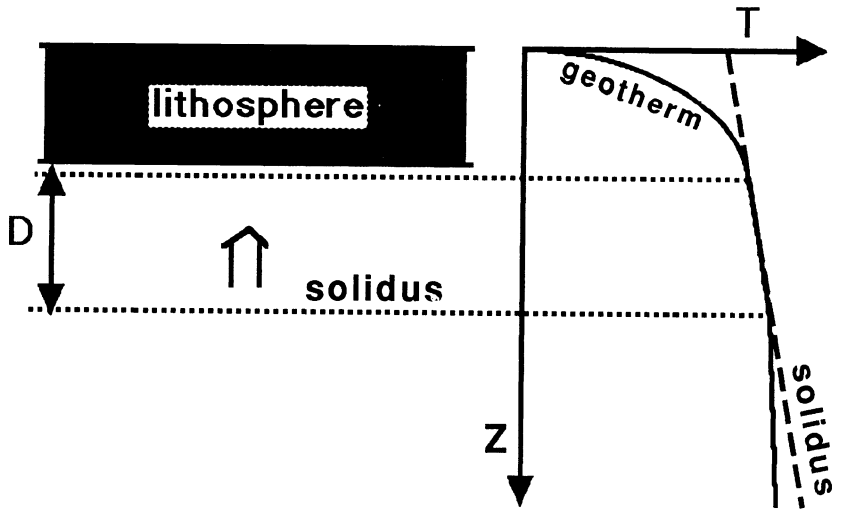

Figure 1. Initial condition. On the left is a cross-section through the lithosphere and asthenosphere, and on the right is the corresponding temperature profile, with the solidus indicated (dashed lines). D is the most important length scale.

The layer of rock at the solidus, which may be either partially molten or on the onset of melting, is unstable to a Rayleigh-Taylor like instability as follows: If an element of rock is given an infinitesimal velocity upwards, it will experience pressure-release partial melting, and hence a decrease in density since the melt (and possibly the solid residuum - see section 2.3) is less dense than the solid. The resulting buoyancy causes increased upwelling velocity and a higher rate of melting, a positive feedback situation which can lead to an episode of circulation, magma production and possibly surface magmatism. Since the degree of partial melting and hence buoyancy is proportional to the vertical distance moved, the growth of velocity is exponential, as in a conventional Rayleigh-Taylor instability at early times (Turcotte and Schubert, 1982).

2.2. EFFECT OF MELT MIGRATION

The situation is made more complicated by migration of melt by percolation through the solid matrix. Since melt buoyancy drives the bulk flow, percolation of melt up and out of the system diminishes the buoyancy and vigor of the flow. Melt percolation can reasonably be described by Darcy's law (McKenzie, 1984; Stevenson and Scott, 1991); arguably the most realistic form in this application is one in which the permeability, k, is proportional to porosity squared. This predicts that the melt velocity relative to solid is proportional to the porosity. The volume flux of melt per unit area of solid is therefore proportional to porosity squared.

Thus, the bulk average upwelling velocity of solid and liquid is linear in melt fraction, and the flux of melt through the solid is quadratic in melt fraction. Since the melting rate is proportional to upwelling velocity, at low melt fractions melting will exceed percolation. Therefore the melt fraction and hence flow velocity will increase, reaching a nearly steady-state at which the melting rate is balanced by percolation.

To get a clear picture of how melt migration affects the dynamics it is instructive to consider limiting cases. In the limit of infinite permeability the melt is removed instantaneously, hence there is no buoyancy, and no bulk flow occurs. In the limit of zero permeability (k=0), the melt fraction, hence buoyancy and circulation velocity, is at its maximum possible value determined by the vertical dimension of the melting region D_{melt}, and the rate of melting of an adiabatically upwelling element, $\partial f/\partial z$:

$$f_{\max} = D_{melt} \frac{\partial f}{\partial z} \Big|_{k=0} \qquad (1)$$

However, in this case no magmatism is observed at the surface.

2.3. COMPOSITIONAL CHANGES

Since it is the denser components, garnet and clinopyroxene, that melt first, the residual solid component is also less dense than the unmelted rock, and provides an additional contribution to the buoyancy. Even in the case of infinite permeability, buoyancy would be present. This effect has been used as a buoyancy source in some models (Mutter et al., 1988). However, the situation is made complicated on Earth by garnet-spinel-plagioclase phase transitions occurring at depths of interest, and by the possible existence of a stably stratified depleted layer at the top of the asthenosphere as a result of mid-ocean ridge melting processes. On

other planets the presence of this buoyancy source is less certain. All these effects have been numerically modelled, but since the aim of this paper is to describe the basic physics in a way which is scalable to different dimensional parameters and different planets, compositional buoyancy is ignored here.

3. Equations and Numerical Model

Three sets of equations are necessary, describing the bulk flow, melt percolation and advection/diffusion.

It is appropriate to nondimensionalise the equations to the vertical dimension of the melting region (D, shown in figure 1), the diffusive timescale (D^2/κ, where κ=thermal diffusivity), the maximum melt fraction (f_{max}, (1)), and the superadiabatic temperature drop across the mobile part of the upper boundary layer (ΔT), which is about 300°C in this case (section 2.1). Nondimensional variables are denoted by tildas.

The bulk flow v of the local center of mass of solid and liquid, assumed to be incompressible and of infinite Prandtl number, is described by mass conservation and the Stokes equation with an extra term describing the buoyancy due to melting:

$$\nabla \bullet \tilde{v} = 0 \tag{2}$$

$$\nabla \tilde{p} - \nabla^2 \tilde{v} = \left(Ra.\tilde{T} + Rm.\tilde{f}\right).\hat{\tilde{z}} \tag{3}$$

where $\tilde{T}$ is the nondimensional temperature, $\tilde{f}$ is the normalized melt fraction and $\tilde{p}$ is the nondimensional pressure. Ra and Rm are the Rayleigh numbers for thermal buoyancy-driven and melt buoyancy-driven flow respectively:

$$Ra = \frac{\rho g \alpha \Delta T D^3}{\eta \kappa} \tag{4}$$

$$Rm = -\frac{g f_{max} D^3}{\eta \kappa} \frac{\partial \rho}{\partial f} \tag{5}$$

where α is the thermal expansivity, η is the asthenospheric viscosity at the depth of onset of melting, κ is the thermal diffusivity, and f_{max} is defined in (1).

A realistic temperature dependent viscosity law is used, so that the lithosphere arises naturally from the equations rather than being artificially imposed.

$$\eta(T) = \eta_o \exp\left(\frac{E_{act}}{RT}\right) \tag{6}$$

R is the gas constant. We use a value of E_{act}, the activation energy, of 420kJ/mole.

The segregation of solid and melt **u**, is described by Darcy's law. We assume melt percolation is in the vertical direction, and porosity is equal to melt fraction.

$$\tilde{\mathbf{u}} = \tilde{f}\left(\tilde{v}_{liq} - \tilde{v}_{sol}\right) = \frac{Rm}{M}(1-f).\tilde{f}^2.\hat{\tilde{z}} \tag{7}$$

where M is the melt retention number:

$$M = \frac{\eta_{liq} D^2}{\eta\, k_0} \tag{8}$$

η_{liq} is the viscosity of the melt, and k_0 is the permeability constant. High values of M correspond to very slow percolation, resulting in vigorous bulk circulation, and low values of M correspond to fast percolation, resulting in slow bulk circulation, as discussed earlier.

The full form of Darcy's law for melt migration problems includes a term related to compaction of the solid matrix. This term is only important on lengths of the order of the compaction length, which is around 0.1-1km for reasonable mantle properties in this case (Stevenson and Scott, 1991). The length scales of interest here are tens of kilometers, so we neglect this term. It is also possible that the permeability is zero below a certain melt fraction threshold of order 1% (Nakano et al., 1989). Since this does not fundamentally alter the physics of the mechanism, in fact slightly favoring the development of these instabilities, we neglect this possibility.

Finally, advection/diffusion equations are required for temperature and melt fraction, f:

$$\frac{\partial \tilde{T}}{\partial \tilde{t}} = \nabla^2 \tilde{T} - \tilde{v}_{sol} \bullet \nabla \tilde{T} - L.\tilde{m} \tag{9}$$

$$\frac{\partial \tilde{f}}{\partial \tilde{t}} = -(1-f)\frac{\partial \tilde{u}}{\partial \tilde{z}} - \tilde{v}_{sol} \bullet \nabla \tilde{f} + \tilde{m} \tag{10}$$

where L is the latent heat, m is the rate of melting, and $\mathbf{v}_{sol} = \mathbf{v}\text{-}\mathbf{u}$ is the velocity of the solid component.

The equations are solved using a Petrov-Galerkin finite element scheme (Hughes, 1987; Hughes et al., 1989) with a varying element size, designed to give maximum resolution at the top of the asthenosphere where it is most needed.

In the lithosphere the mechanism for melt migration changes to one of rapid propagation through cracks. Since this is beyond the scope of the numerical model, melt percolating by Darcy flow in the upper part of the partially molten layer is simply removed, and measured as an 'eruption rate'. In reality only a fraction of this material would erupt at the surface.

4. Results

In order to isolate and study the effects of melt buoyancy, the thermally-driven component to the flow was eliminated by setting α, hence Ra, to zero, and imposing zero heat flux at the lower boundary. Values of Ra appropriate to this situation are probably close to critical (Haxby and Weissel, 1986).

The velocity boundary conditions are impermeable, stress-freeon the base and outside of the box and rigid at the top. The temperature boundary conditions are isothermal at the top, and zero heat-flux at the base. Calculations in larger boxes verified that box is sufficiently large that the limited box size and velocity boundary conditions have negligible effect on the flow, and calculations at higher resolutions verified that the resolution is adequate. The initial push is provided by a temperature perturbation of 0.4% of the total temperature drop (scaling to about 5°C), exponentially decreasing away from the symmetry axis. This temperature perturbation is immediately converted into partial melt.

4.1. TYPICAL SIMULATIONS

Figure 2 show a typical simulation for the values $Rm=10^5(=100k)$, M=150. Time is normalized to the diffusive timescale D^2/κ, which is about 50Ma for D=40km. The four frames show the growth, peak, decline and death of the circulation. The circulation dies out for two reasons. Firstly, some of the depleted and cooled material that has already upwelled once gets recirculated into the upwelling. This material cannot contribute to the buoyancy, and so has the effect of progressively pinching off the upwelling. Secondly, the system as a whole is undergoing cooling, particularly near the base of the viscous lithosphere. Thus the viscous lithosphere thickens, reducing D and hence M and Rm. Cooling also causes increased viscosity in dry areas of the asthenosphere, further diminishing the flow.

The time evolution of bulk flow velocity and eruption rate are shown in figure 3 for three cases. Velocity, time and eruption rate are nondimensionalised to thermal quantities, κ/D, D^2/κ and κD respectively (about 0.1cm/yr, 50Ma and 1300km^3/Ma for D=40km, $\kappa=10^{-6}$m^2/s). In each case the rapid rise, leading to a long, gradually decreasing plateau, and a fairly rapid dying out, are apparent. The growth of the velocity with time looks linear on this semi-logarithmic plot, confirming that the growth is indeed exponential. The time lag between the velocity curve and the eruption curve is indicative of the melt percolation time through the layer.

The three cases shown are a reference case ($Rm=50k=5.10^4$, M=150), one with Rm doubled, which corresponds to figure 2 (Rm=100k, M=150), and one with M increased by an order of magnitude (Rm=50k, M=1500). The effect of doubling Rm is, to first order, a doubling of nondimensional velocity with the nondimensional timescale remaining constant. Increasing M increases both the flow velocity and timescale.

4.2. EFFECT OF PARAMETERS

The effect of the main parameters Rm, M and D on the length scale, timescale and eruption rates are now investigated more thoroughly. All results are nondimensionalised to thermal quantities, as described above.

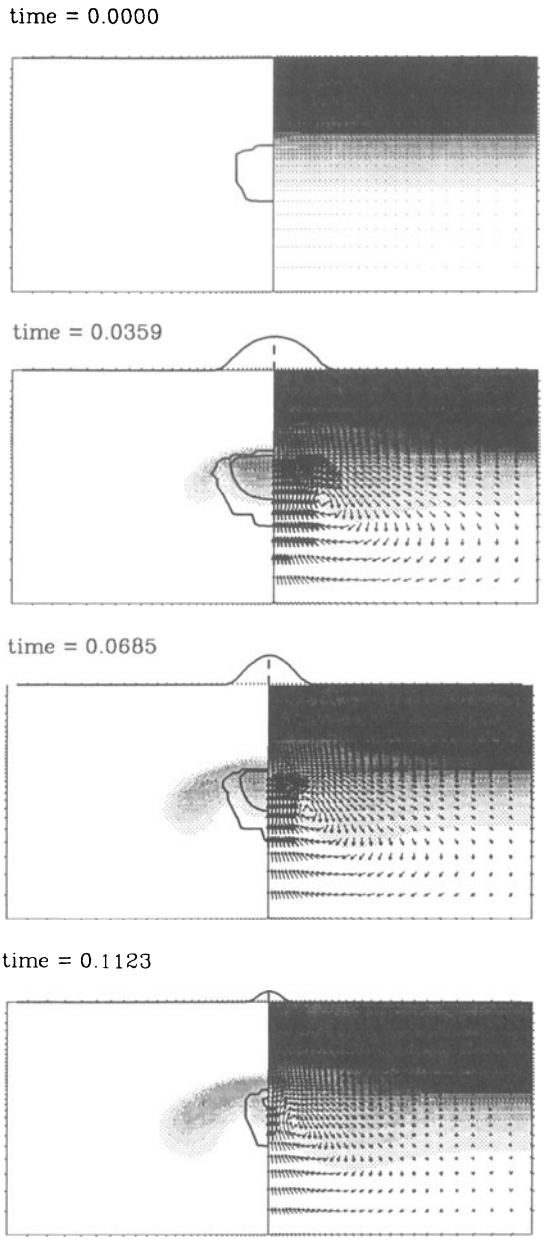

Figure 2. Simulation for Rm=100k, M=150, Ra=0, in axisymmetric geometry, at four times showing start, peak, decline and death of the instability. Each frame shows temperature (right, shaded), velocity (right, arrows), melt fraction (left, contours at 0 and intervals of 2.5%), composition (left, shaded means depleted), and eruption rate per unit area (graph on top). Dimensions of box are 3.25D and 2.75D, initial lithospheric thickness is D.

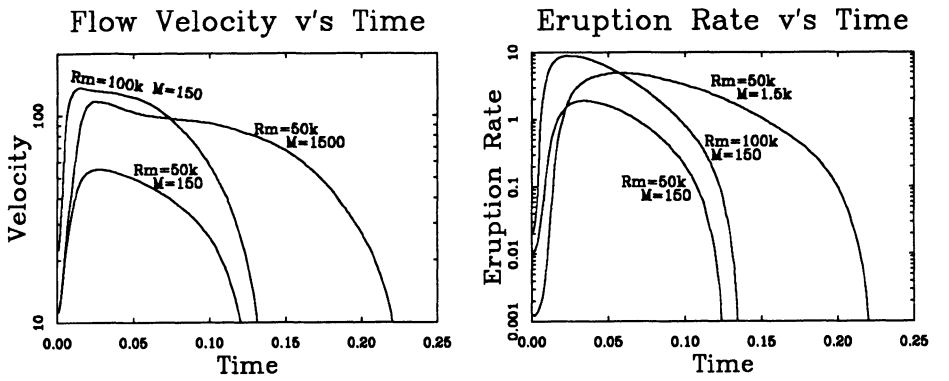

Figure 3. Time evolution of velocity and eruption rate for three cases. Time, velocity and eruption rate are nondimensionalized to D^2/κ, κ/D and κD respectively.

4.2.1. *Length scale.* Drawing an analogy between this instability and the classical Rayleigh-Taylor instability between two highly viscous fluids of different densities bounded by upper and lower boundaries (Turcotte and Schubert, 1984), the preferred spacing of upwellings is expected to be determined solely by the vertical length scale, D.

To determine this preferred spacing, numerical experiments were performed in long Cartesian boxes with random initial temperature perturbations. A typical result, in an aspect ratio 4 box with impermeable boundary conditions, is shown in figure 4. The initial random temperature perturbations are of amplitude 0.4% the total temperature drop, as before. After a short time, five upwellings have formed, two of them being strong, and three weak. In general, experiments at this aspect ratio lead to between three and five upwellings, indicating that the preferred number is about four, corresponding to a spacing of 2.5xD. This preferred spacing is also observed with other aspect ratios.

4.2.2 *Timescale.* Figure 5 a) and b) shows the effect of Rm and M on the nondimensional timescale, defined as the elapsed time between the start of the simulation and the point at which the melt fraction and velocity are zero everywhere.

The timescale is approximately constant for Rm > 50k, decreasing rapidly at low values. However it increases significantly with increasing M, beginning to saturate at about $M=10^5$.

4.2.3. *Peak Velocity and Eruption Rates.* The effect of Rm and M on the peak velocity is shown in figure 5 c) and d). The relationship between peak velocity and Rm appears linear, except at low Rm values where thermal diffusion becomes important. The peak velocity increases steadily with M until it saturates at about $M=10^4$.

Similar curves for eruption rate, averaged over the lifetime of the system, are shown in figure 5e) and f). The eruption rate, like the velocity, appears approximately linear in Rm. However, in M-space the eruption rate reaches a peak at around $M=10^3$, and declines rapidly either side of this.

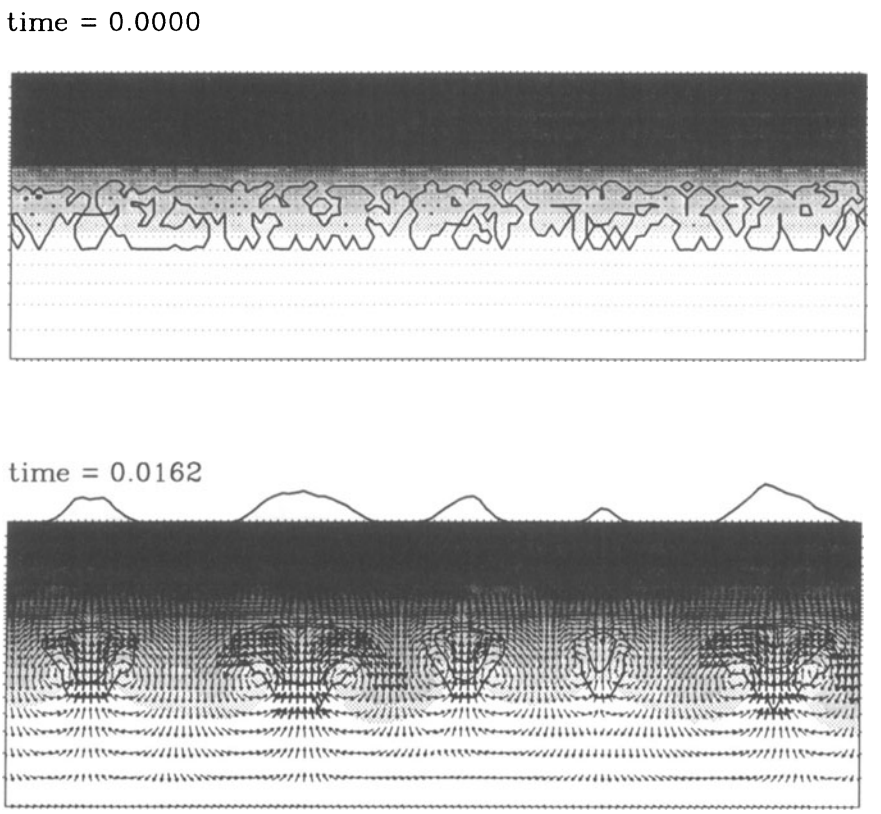

Figure 4. Simulation in a 4x1 cartesian box for Rm=50k, M=150, Ra=0. Upper plot shows random initial condition, lower plot shows subsequent development of upwellings. Temperature (shaded), velocity (arrows), melt fraction (contours) and eruption rate (graph), as figure 2.

5. Discussion

5.1. INTERPRETATION OF PARAMETERS

The results in the previous section lead to a qualitative interpretation of the main parameters.

Rm may be interpreted as $V_{stokes}/V_{thermal}$, where V_{stokes} is the characteristic velocity induced by melt buoyancy, derived by dimensional analysis from the Stokes equation, and $V_{thermal}$ is the same from the energy equation. Although one can interpret the thermal Rayleigh number Ra in the same way (except with thermal buoyancy), there is an important difference between the buoyancy forces in each case: in melt-driven flow, the buoyancy of an element increases as it rises, but in thermally-driven flow within an otherwise adiabatic region, the buoyancy remains constant.

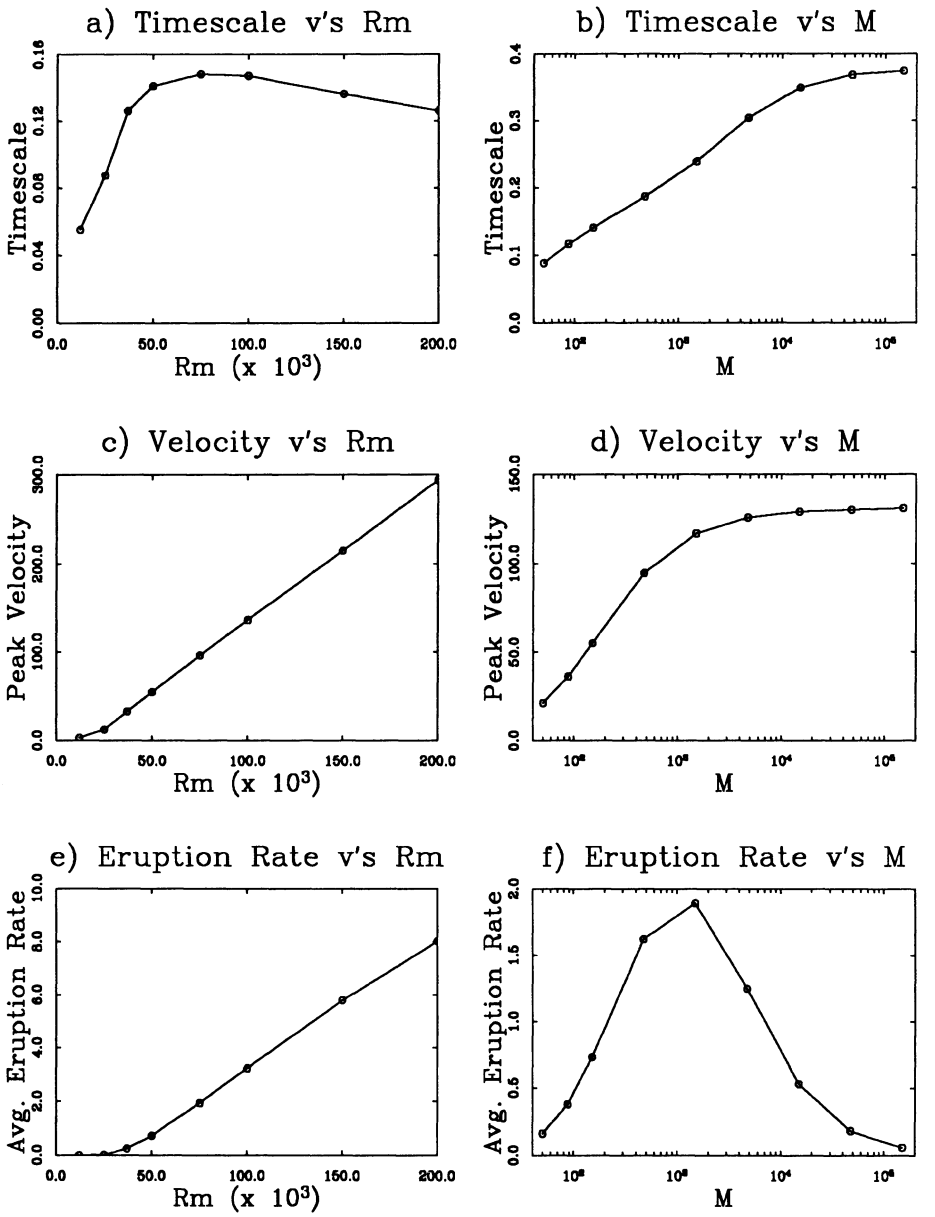

Figure 5. Effect of Rm and M on timescale, velocity and eruption rate. In a) c) and e) M is fixed at 150, in b), d) and f) Rm is fixed at 50k. Time, velocity and eruption rate. nondimensionalized to D2/κ, κ/D and κD respectively.

Rm primarily affects the nondimensional peak velocity and average eruption rate in an approximate proportionality, and has little effect on the nondimensional timescale except at low values. At these low values, thermal cooling becomes comparable with advection of heat, particularly during the early growth of the instability when the thermal velocity may exceed the flow velocity, and so the size of the initial perturbation becomes important. In the low Rm limit, thermal cooling dominates advection of heat, and the observed activity is simply due to relaxation of the initial condition.

M may be interpreted as V_{stokes}/V_{melt}, and in a sense is closer to the thermal Rayleigh number in physical meaning than Rm is, since both M and Ra are the ratio of flow velocity to the velocity at which the buoyancy force is dissipating. It affects the peak velocity and the timescale in a similar way, both increasing steadily with M and then saturating at high M. However, the eruption rate increases with M, then decreases. The effect on velocity can be understood as follows: In the limit of zero permeability (M=infinity) the maximum possible peak flow velocity, determined by Rm, is obtained; at finite M the buoyancy is reduced due to melt percolation and only some fraction of this velocity is reached. The effect on the timescale is due to the presence of melt buffering the system against cooling: melt fraction and thus timescale increase with increasing M. The eruption rate is low for high M because it is related to the percolative flux of melt at the top of the asthenosphere, and at high M the permeability and hence flux is small. At low M the eruption rate follows the trend of the velocity and other indicators of activity.

5.2. INITIAL STATE

In a partially molten layer where the temperature is buffered at the solidus, infinitesimal perturbations will grow exponentially into significant flow, so that these instabilities will develop spontaneously, as in the classical Rayleigh-Taylor instability (Turcotte and Schubert, 1984). In this case the instability greatly amplifies the amount of melt available for magmatism.

If the temperature is merely close to the solidus, then a vertical "push" is required to initiate melting and melt-driven flow. The required "push" could be provided by local small-scale flow, for example thermally-driven flow (Buck and Parmentier, 1986; Haxby and Weissel, 1986; Richter and Parsons, 1975), flow induced by fracture zones (Robinson et al., 1988), and passive corner-flow circulation induced at spreading centers. Hence a pervasively partially-molten asthenosphere is not required for these instabilities to develop.

5.3. INTERACTION WITH OTHER SMALL-SCALE FLOW

Simulations which include thermal buoyancy indicate that the melt-driven flow, once induced, can dominate thermally-driven flow. Even at lower values of M and Rm, melt buoyancy is observed to have a significant effect on the thermally-driven flow. The interaction between the two driving forces can result in a richness of phenomena not observed by treating each force separately. Thus, to correctly model flow in the asthenosphere it is necessary to include melt buoyancy.

5.4. VOLCANO SPACING

Characteristic spacing of major volcanic centers is observed in many situations, for example along hotspot chains. One current theory explains this by invoking stresses in the lithosphere (ten Brink, 1991). However, in the results presented in section 4.2.1, upwellings exhibit a characteristic spacing related to D, the vertical distance between the onset of melting and the base of the viscous lithosphere. Thus, fluid dynamics in the asthenosphere provides an alternative explanation for the spacing observed in nature. One upwelling may correspond to one volcano or a cluster of volcanoes, depending on the details of crack dynamics in the lithosphere.

5.5. LITHOSPHERIC EROSION

Melting of the rock as it rises adiabatically is accomplished by the absorption of latent heat by the melt. The subsequent vertical percolation of the melt to the top of the partially molten layer is effectively transporting this latent heat energy upwards, enhancing the vertical heat transport. In the calculations presented in this paper, much of this melt was removed from the top of the layer, removing the energy from the system. Calculations in which all the melt is allowed to freeze at the top of the asthenosphere, releasing its latent heat, indicate considerable thinning or erosion of the viscous lithosphere on timescales much shorter than predicted by diffusion alone.

The exact mechanism for this is as follows: The presence of partial melt at the top of the asthenosphere effectively buffers the temperature to the solidus temperature. The entire partially molten layer is being advected upwards by the bulk circulation described by Stokes equation. Thermal diffusion is important on small length scales near the top of the partially molten region, warming and hence softening the base of the viscous lithosphere, allowing further upward movement by Stokes flow. While melt is being supplied to the top of the layer by Darcy flow, Stokes flow and pressure-release melting at a faster rate than it is freezing due to thermal conduction, the lithosphere will thin. This combination of diffusion on small length scales and advection causes much faster erosion than thermal diffusion alone. Since the erosion timescale is much less than the corresponding diffusion timescale, a non-equilibrium lithospheric temperature profile results.

Preliminary results suggest that lithospheric thinning by a factor of up to two in a few million years may be possible. Due to difficulty in resolving the high thermal, viscosity and compositional gradients resulting from the non-equilibrium temperature profile, further investigation is needed to validate these numerical results.The situation is further complicated by the possibility of a high melt-fraction compaction layer at the base of the lithosphere (Sparks and Parmentier, 1991).

5.6. OCEANIC SEAMOUNTS

There are a large number of oceanic seamounts, which have been particularly well studied in the Pacific Ocean. Batiza (1982) estimated that there are 22-55,000 >1km high seamounts on the Pacific floor, and Smith and Jordan (1988) estimate roughly one million of all sizes. Smith and Jordan's analysis suggests that 78% of the large (>1km high) non-hotspot, non-fracture zone seamounts were formed away from the axis of the East Pacific spreading center,

on lithosphere that was already up to several tens of Ma old. Examples of seamounts produced off-axis are described by Honda et al. (1987).

There is much uncertainty in the values of parameters appropriate to young oceanic asthenosphere, particularly in η and k_0. However, Rm and M are most sensitive to D. The depth of onset of melting for n-type Mid-Ocean Ridge Basalt (MORB) has been calculated to be at around 80km (McKenzie and O'Nions, 1991). Taking reasonable parameters: $\eta=10^{18}$Pa.s, η_{liq}=10Pa.s, $d\rho/df$=-500kg/m^3, $k_0=3\times10^{-10}$m^2, D=30-50km, we obtain Rm=20-74k and M=31-90. Scaling the numerical results to this dimensional space, we obtain flow velocities of up to ~10cm/yr, timescales of ~10Ma, spacings of ~100km, and magma production rates of up to ~1500 km^3/Myr. The total magma volume can be several times that required to build the largest seamounts, and the observed seamount volume per unit area in the Pacific (Smith and Jordan, 1989). Thus, the mechanism provides a plausible explanation for oceanic seamounts. The fertile asthenospheric material would be provided by rock which is drawn up by the mid-ocean ridge corner-flow but misses the proposed focussed upwelling directly under the ridge (Buck and Su, 1989; Scott and Stevenson, 1989). Some distance from the ridge, there is still a vertical component to the velocity, leading to the temperature profile in figure 1. Each upwelling may feed several volcanoes, the number being determined by cracks in the lithosphere, and the height determined by the depth of the feeding magma chamber, related perhaps to the thickness of the lithosphere.

5.7. LARGER VOLCANOES

Where anomalously high asthenospheric temperatures exist, for example where material has been emplaced by a plume, the depth of onset of melting may be much deeper than 80km; McKenzie and O'Nions (1991) calculate 120km for e-type MORB. Using D=50-90km and otherwise the same parameters as in section 5.6, we obtain Rm=74-430k, M=90-290. The numerical results scale to flow velocities of ~10-20 cm/yr, timescales of 10-40 Ma, eruption rates of ~1000-40000 km^3/Ma, and spacings of 125-200km. Thus, this mechanism may be important in the dynamics of such regions.

6. Conclusions

We have presented a model for self-perpetuating, melt-buoyancy-driven asthenospheric flow and volcanism arising from Rayleigh-Taylor instabilities in the asthenosphere. The mechanism can generate surface volcanism without a deep source, such as a plume. In the presence of pre-existing small-scale circulation, the instability can be triggered without a pervasively partially-molten asthenosphere. The important parameters are the melt-buoyancy Rayleigh number Rm, the melt retention number M, and the vertical distance between the onset of melting and the base of the viscous lithosphere, D: the time scale is determined mainly by M and the amount of magmatism by M and Rm.

The melt-driven upwellings exhibit a characteristic spacing proportional to D. This may provide an explanation for the frequently observed characteristic spacing of volcanic centers.

If a large fraction of the melt generated freezes at the base of the viscous lithosphere rather than erupting, then significant lithospheric thinning is possible.

When scaled to parameters realistic to young oceanic lithosphere, the magma volumes produced and timescales are compatible with observations of intra-plate volcanism, in

particular the tens of thousands of large seamounts in the Pacific which appear unrelated to major hotspot chains.

Melt buoyancy can have a major effect on asthenospheric dynamics. Flow resulting from the interaction of thermal buoyancy and melt buoyancy exhibits greater complexity than flow driven by either of these individually. Hence, it is important to consider partial melting when studying the dynamics of the asthenosphere.

Acknowledgments. We are grateful to David Scott for furnishing us with his finite element code. We thank Don Anderson for a thoughtful review of the manuscript and helpful suggestions, and Craig Scrivner and Helen Qian for improving the quality of the text. The work benefitted from discussions with Geoff Davies. Supported by NSF grant EAR9017893. Contribution Number 5147, Division of Geological and Planetary Sciences, California Institute of Technology, Pasadena, CA 91125.

7. References

Batiza, R. (1982) Abundances, distribution and sizes of volcanos in the Pacific Ocean and implications for the origin of non-hotspot volcanoes, Earth Plan. Sci. Lett., 60, 195-206.

Boss, A.P. and Sacks, I.S. (1985) Formation and growth of deep mantle plumes, Geophys. J.R. Astr. Soc., 80, 241-255.

ten Brink, U. (1991) Volcano spacing and plate rigidity, Geology, 19, 397-400.

Buck, W.R. and Parmentier, E.M. (1986) Convection beneath young oceanic lithosphere: Implications for thermal structure and gravity, J. Geophys. Res., 49, 1961-1974.

Buck, W.R. and Su, W. (1989) Focussed mantle upwelling below mid-ocean ridges due to feedback between viscosity and Melting, Geophys. Res. Lett., 16, 641-644.

Griffiths, R.W. (1986) Dynamics of mantle thermals with constant buoyancy or anomalous internal heating, Earth Plan. Sci. Lett., 78, 435-446.

Haxby, W.F. and Weissel, J.K. (1986) Evidence for small-scale mantle convection from seasat altimeter data, J. Geophys. Res., 91, 3507-3520.

Honda, M., Bernatowicz, T., Podosek, F.A., Batiza, R. and Taylor, P.T. (1987) Age determinations of eastern pacific seamounts (Henderson, 6 and 7) - implications for near-ridge and intraplate volcanism, Marine Geology, 74, 79-84.

Hughes, T.J.R. (1987) The Finite Element Method, Prentice-Hall, Englewood Cliffs NJ, 631pp.

Hughes, T.J.R., Liu, W.K. and Brooks, A. (1979) Finite element analysis of incompressible viscous flows by the penalty function formulation, J. Comput. Phys., 30, 19-35.

Kellogg, L.H. (1991) Interaction of plumes with a compositional boundary at 670km, Geophys. Res. Lett., 18, 865-868.

Liu, M., Yuen, D.A. and Honda, S. (1991) Development of diapiric structures in the upper mantle due to phase transitions, Science 252, 1836-1839.

McKenzie, D.P. (1984) The generation and compaction of partially molten rock, J.Petrol., 25, 713-765.

McKenzie, D.P. and O'Nions, R.K. (1991) Partial melt distributions from inversion of rare earth element concentrations, in press, J. Petrol.

Nakano, T. and Fuji, N. (1989) The multiphase grain control percolation: Its implication for a partially molten rock, J. Geophys. Res., 94, 15653-15661.

Olson, P., Schubert, G. and Anderson, C. (1987) Plume formation in the D" layer and the roughness of the core-mantle boundary, Nature, 327, 409-413.

Richards, M.A. and Griffiths, R.W. (1988) Deflection of plumes by mantle shear flow: experimental results and a simple theory, Geophys. J., 94, 367-376.

Richter, F.M. and Parsons, B. (1975) On the interaction of two scales of convection in the mantle, J. Geophys. Res., 80, 2529-2541.

Robinson, E.M., Parsons, B. and Driscoll, M. (1988) The effect of a shallow low-viscosity zone on the mantle flow, the geoid anomalies and depth-age relationships at fracture zones, Geophys. J., 93, 25-43.

Scott, D.R. and Stevenson, D.J. (1989) A self-consistent model of melting, magma migration and buoyancy-driven circulation beneath mid-ocean ridges, J. Geophys. Res., 94, 2973-2988.

Smith, D.K. and Jordan, T.H. (1988) Seamount statistics in the pacific ocean, J. Geophys. Res., 93, 2899-2918.

Sparks, D.W. and Parmentier, E.M. (1991) Melt extraction from the mantle beneath spreading centers, in press, Earth Plan. Sci. Lett.

Stevenson, D.J. (1988) Rayleigh-Taylor instabilities in partially molten rock, EOS, 69, 1404.

Stevenson, D.J. and Scott, D.R. (1991) Mechanics of Fluid-Rock systems, Annual Reviews of Fluid Mechanics, 23, 305-339.

Turcotte, D.L. and Schubert, G. (1982) Geodynamics, John Wiley and Sons, New York, pp. 251-257.